Dynamic turbulence modelling in large-eddy simulations of the cloud-topped atmospheric boundary layer

By M. P. Kirkpatrick, N. N. Mansour, A. S. Ackerman †, and D. E. Stevens ‡

1. Motivation and Objectives

The use of large eddy simulation, or LES, to study the atmospheric boundary layer dates back to the early 1970s when Deardorff (1972) used a three-dimensional simulation to determine velocity and temperature scales in the convective boundary layer. In 1974 he applied LES to the problem of mixing layer entrainment (Deardorff 1974) and in 1980 to the cloud-topped boundary layer (Deardorff 1980*b*). Since that time the LES approach has been applied to atmospheric boundary layer problems by numerous authors.

While LES has been shown to be relatively robust for simple cases such as a clear, convective boundary layer (Mason 1989), simulation of the cloud-topped boundary layer has proved more of a challenge. The combination of small length scales and anisotropic turbulence coupled with cloud microphysics and radiation effects places a heavy burden on the turbulence model, especially in the cloud-top region. Consequently, over the past few decades considerable effort has been devoted to developing turbulence models that are better able to parameterise these processes. Much of this work has involved taking parameterisations developed for neutral boundary layers and deriving corrections to account for buoyancy effects associated with the background stratification and local buoyancy sources due to radiative and latent heat transfer within the cloud (see Lilly 1962; Deardorff 1980*a*; Mason 1989; MacVean & Mason 1990, for example). In this paper we hope to contribute to this effort by presenting a number of turbulence models in which the model coefficients are calculated dynamically during the simulation rather than being prescribed *a priori*.

The dynamic procedure, first proposed by Germano *et al.* (1991), computes model coefficients using information contained in the resolved velocity and scalar fields. In this sense dynamic models can be considered self-calibrating, a feature that makes them an appealing choice for dealing with the complex interactions between the hydrodynamics, radiation and cloud microphysics occurring within clouds. Nevertheless, while dynamic turbulence models have been used with considerable success for complex engineering flows (see Boivin *et al.* 2000; Branley & Jones 2001, for example), their application to atmospheric flows has been very limited.

The objective of this paper is to present a set of dynamic turbulence models written in a form appropriate for large eddy simulations of the atmospheric boundary layer in which the flow is described using equations of motion in anelastic form . The models are tested using simulations of a nocturnal marine stratocumulus cloud observed during during the second Dynamics and Chemistry of Marine Stratocumulus (DYCOMS-II) field experiment. This test case includes a number of features that typically cause problems

† NASA Ames, Earth Science Division
‡ Lawrence Livermore National Laboratory

in simulations of the atmospheric boundary layer, including the presence of a strong temperature inversion at the level of the cloud top, and positive feedback loops involving turbulent entrainment across the inversion, radiation and cloud microphysics. As such, these simulations provide a good test for the utility of our models. Simulations are performed using the atmospheric boundary layer LES code, DHARMA, (Stevens & Bretherton 1999; Stevens *et al.* 2000), with dynamic turbulence models computed using the new LLAMA code presented here.

2. Dynamic turbulence models for the anelastic equations

The dynamics of the cloud-topped atmospheric boundary layer can be described using equations for conservation of mass, momentum, liquid water potential temperature and total water mixing ratio. These equations are written in the anelastic form of Ogura & Phillips (1962) in which the thermodynamic variables such as pressure p are decomposed into an isentropic base state p_0 (corresponding to a uniform potential temperature θ_0) and a dynamic component. Following Clark (1979), the dynamic component is further decomposed into an initial environmental deviation in hydrostatic balance p_1 and a time-evolving dynamic perturbation p_2 to give

$$p(x, y, z, t) = p_0(z) + p_1(z) + p_2(x, y, z, t). \tag{2.1}$$

After subtracting hydrostatic balances, the resulting continuous equations are written,

$$\frac{\partial \varrho_0 u_i}{\partial t} + \frac{\partial (\varrho_0 u_i u_j)}{\partial x_j} = -\frac{\partial p_2}{\partial x_i} + \delta_{i3} g \frac{\varrho_0 \theta_{v2}}{\theta_0} - \epsilon_{ijk} \varrho_0 f_j u_k + H_{u_i}, \tag{2.2}$$

$$\frac{\partial \varrho_0 \theta_l^*}{\partial t} + \frac{\partial (\varrho_0 \theta_l^* u_j)}{\partial x_j} = H_{\theta_l^*}, \tag{2.3}$$

$$\frac{\partial \varrho_0 q_t}{\partial t} + \frac{\partial (\varrho_0 q_t u_j)}{\partial x_j} = H_{q_t}, \tag{2.4}$$

$$\frac{\partial (\varrho_0 u_j)}{\partial x_j} = 0. \tag{2.5}$$

Here u_i are the Cartesian components of the velocity vector, ϱ the density, δ_{ij} the Kronecker delta, ϵ_{ijk} the permutation tensor, f_j the Coriolis parameter, g the acceleration due to gravity, q_t the total water mixing ratio and $\theta_l^* = (\theta_l - \theta_0)/\theta_0$ a scaled liquid water potential temperature. Total water mixing ratio is the sum of the liquid and vapour mixing ratios,

$$q_t = q_c + q_v = \frac{\varrho_c + \varrho_v}{\varrho_d}, \tag{2.6}$$

where ϱ_c, ϱ_v and ϱ_d are the density of the condensed water, water vapour and dry air respectively. Liquid water potential temperature is defined as

$$\theta_l = \theta - \frac{L q_c}{C_{pd} \pi_0}. \tag{2.7}$$

Here L is the latent heat of vaporisation, C_{pd} the specific heat at constant pressure for dry air and $\pi_0 = \left(\frac{p_0}{p_{ref}}\right)^{\frac{R_d}{C_p}}$ with p_{ref} a reference pressure and R_d the gas constant of dry air. The virtual potential temperature θ_v appearing in the buoyancy term of the

momentum equations is given by

$$\theta_v = \theta + \theta_0 \left[\left(\frac{R_d}{R_v} - 1 \right) q_v - q_c \right], \tag{2.8}$$

where R_v is the gas constant for water vapour. The terms H_{u_i}, $H_{\theta_l^*}$ and H_{q_t} are source terms that include parameterisations for physical processes such as radiation, precipitation and the effects of the global atmospheric circulation.

In a large eddy simulation, the equations are filtered to remove from the solution those fluctuations that cannot be resolved by the numerical method. For the anelastic equations it is convenient to use a density-weighted or Favre filter, where a Favre filtered variable is defined as $\widetilde{\phi} = \overline{\varrho\phi}/\overline{\varrho}$. Application of this filter to the equations gives

$$\frac{\partial \overline{\varrho}_0 \widetilde{u}_i}{\partial t} + \frac{\partial (\overline{\varrho}_0 \widetilde{u}_i \widetilde{u}_j)}{\partial x_j} = -\frac{\partial \overline{p}_2}{\partial x_i} + \delta_{i3} g \frac{\overline{\varrho}_0 \widetilde{\theta}_{v2}}{\theta_0} - \epsilon_{ijk} \overline{\varrho}_0 \widetilde{u}_k f_j + H_{u_i} - \frac{\partial \tau_{ij}}{\partial x_j}, \tag{2.9}$$

$$\frac{\partial \overline{\varrho}_0 \widetilde{\theta}_l^*}{\partial t} + \frac{\partial (\overline{\varrho}_0 \widetilde{\theta}_l^* \widetilde{u}_j)}{\partial x_j} = H_{\theta_l^*} - \frac{\partial \gamma_{\theta_l^*}}{\partial x_j}, \tag{2.10}$$

$$\frac{\partial \overline{\varrho}_0 \widetilde{q}_t}{\partial t} + \frac{\partial (\overline{\varrho}_0 \widetilde{q}_t \widetilde{u}_j)}{\partial x_j} = H_{q_t} - \frac{\partial \gamma_{q_t}}{\partial x_j}, \tag{2.11}$$

$$\frac{\partial (\overline{\varrho}_0 \widetilde{u}_j)}{\partial x_j} = 0, \tag{2.12}$$

with subgrid scale stresses and fluxes given by

$$\tau_{ij} = \overline{\varrho}_0 \left(\widetilde{u_i u_j} - \widetilde{u}_i \widetilde{u}_j \right), \tag{2.13}$$

$$\gamma_{\theta_l^*} = \overline{\varrho}_0 \left(\widetilde{\theta_l^* u_j} - \widetilde{\theta}_l^* \widetilde{u}_j \right), \tag{2.14}$$

$$\gamma_{q_t} = \overline{\varrho}_0 \left(\widetilde{q_t u_j} - \widetilde{q}_t \widetilde{u}_j \right). \tag{2.15}$$

We have assumed here that f_j is constant so that the Coriolis term is linear - an assumption that is valid when the domain is small compared to the Rossby radius of deformation. The source terms H are shown without an overbar since they are parameterisations rather than exact terms.

The Smagorinsky model (Smagorinsky 1963) for the subgrid scale stress is

$$\tau_{ij}^a = \tau_{ij} - \frac{1}{3} \delta_{ij} \tau_{kk} = -2 \overline{\varrho}_0 K_m \widetilde{D}_{ij} C_B, \tag{2.16}$$

where $\widetilde{D}_{ij}$ is the strain rate tensor,

$$\widetilde{D}_{ij} = \frac{1}{2} \left(\frac{\partial \widetilde{u}_i}{\partial x_j} + \frac{\partial \widetilde{u}_j}{\partial x_i} \right) - \frac{1}{3} \delta_{ij} \frac{\partial \widetilde{u}_k}{\partial x_k}. \tag{2.17}$$

Here and elsewhere in this paper the superscript ^{a} is used to denote the anisotropic part of a tensor. The eddy viscosity K_m is given by

$$K_m = C \Delta^2 \left| \widetilde{D} \right|, \tag{2.18}$$

with $\left| \widetilde{D} \right| = \sqrt{2 \widetilde{D}_{ij} \widetilde{D}_{ij}}$ and C a dimensionless coefficient. Stratification effects are ac-

counted for using the correction of Lilly (1962),

$$C_B = (1 - Ri_{sgs})^{1/2} \qquad Ri_{sgs} < 1 \tag{2.19}$$

$$C_B = 0 \qquad Ri_{sgs} \geq 1, \tag{2.20}$$

where the subgrid scale flux Richardson number is estimated using

$$Ri_{sgs} = \frac{g/\theta_0 \, \partial\widetilde{\theta}_v/\partial z}{Pr_{sgs}|\widetilde{D}|^2}. \tag{2.21}$$

Pr_{sgs} is the subgrid scale turbulent Prandtl number, which we set to a constant value of $Pr_{sgs} = 0.4$.

The mixed model of Bardina *et al.* (1983), combines the Smagorinsky model with the scale similarity model of Bardina *et al.* (1980). The model is derived by rewriting the subgrid scale stress tensor in terms of resolved and unresolved parts of the velocity field $u_i = \widetilde{u}_i + u_i'$ using the decomposition of Germano (1986). For the anelastic equations this decomposition takes the form

$$\tau_{ij} = L_{ij}^* + C_{ij}^* + R_{ij}^*, \tag{2.22}$$

where the modified Leonard, cross and SGS Reynolds terms are

$$L_{ij}^* = \overline{\varrho}_0(\widetilde{\widetilde{u}_i\widetilde{u}_j} - \widetilde{\widetilde{u}}_i\widetilde{\widetilde{u}}_j) \tag{2.23}$$

$$C_{ij}^* = \overline{\varrho}_0(\widetilde{\widetilde{u}_i u'}_j + \widetilde{u_i'\widetilde{u}}_j - \widetilde{\widetilde{u}}_i\widetilde{u'}_j - \widetilde{u'}_i\widetilde{\widetilde{u}}_j) \tag{2.24}$$

$$R_{ij}^* = \overline{\varrho}_0(\widetilde{u_i' u'}_j - \widetilde{u'}_i\widetilde{u'}_j). \tag{2.25}$$

The modified Leonard term, which contains only resolved scale quantities, can be calculated explicitly leaving the modified cross and SGS Reynolds terms to be parameterised using the Smagorinsky model,

$$\tau_{ij} = L_{ij}^* - 2\overline{\varrho}_0 C\Delta^2 \left|\widetilde{D}\right| \widetilde{D}_{ij} C_B. \tag{2.26}$$

Martin *et al.* (2000) note that, with the mixed model, the isotropic part of the subgrid scale stress τ_{ij} can be represented at least partially by the isotropic part of the modified Leonard term. In fact they obtained the closest agreement with experiment for their compressible flow test cases when they assumed that the isotropic part of L_{ij}^* models the whole of $\frac{1}{3}\delta_{ij}\tau_{kk}$. We have adopted the same approach in Eq.(2.26).

In dynamic versions of these models, the model coefficient C is calculated dynamically. To achieve this, a test filter is applied to the velocity and scalar fields to extract information from the smallest resolved scales. Application of a spatial test filter (denoted here by a caret) to the filtered momentum equations gives

$$\frac{\partial\widehat{\overline{\varrho}_0\widetilde{u}_i}}{\partial t} + \frac{\partial(\widehat{\overline{\varrho}_0\widetilde{u}_i\widetilde{u}_j})}{\partial x_j} = -\frac{\partial\widehat{\overline{p}_2^*}}{\partial x_i} + \delta_{i3}g\frac{\widehat{\overline{\varrho}_0\widetilde{\theta}_{v2}}}{\theta_0} - \epsilon_{ijk}\widehat{\overline{\varrho}_0\widetilde{u}_k}f_j + H_{u_i} - \frac{\partial\widehat{\tau}_{ij}}{\partial x_j}. \tag{2.27}$$

In order to rewrite this equation in a form similar to Eq.(2.9) we adopt a Favre test filter $\breve{\phi} = \widehat{\varrho\phi}/\widehat{\varrho}$ giving

$$\frac{\partial\widehat{\overline{\varrho}}_0\breve{\widetilde{u}}_i}{\partial t} + \frac{\partial(\widehat{\overline{\varrho}}_0\widetilde{u}_i\breve{\widetilde{u}}_j)}{\partial x_j} = -\frac{\partial\widehat{\overline{p}_2^*}}{\partial x_i} + \delta_{i3}g\frac{\widehat{\overline{\varrho}}_0\breve{\widetilde{\theta}}_{v2}}{\theta_0} - \epsilon_{ijk}\widehat{\overline{\varrho}}_0\breve{\widetilde{u}}_k f_j + H_{u_i} - \frac{\partial\widehat{\tau}_{ij}}{\partial x_j}. \tag{2.28}$$

Since density varies only in the z direction, this equation can be simplified considerably

by using two-dimensional horizontal test filter rather than a three-dimensional one. The Favre test filter is then equivalent to a spatial test filter,

$$\breve{\widehat{\phi}} \equiv \widehat{\widehat{\phi}}, \tag{2.29}$$

and the density field is unchanged by the test filtering operation, that is,

$$\widehat{\widehat{\varrho}}_0 = \overline{\varrho}_0. \tag{2.30}$$

From Eqs.(2.29) and (2.30), with horizontal test filtering Eq.(2.28) becomes

$$\frac{\partial \overline{\varrho}_0 \widehat{\widehat{u}}_i}{\partial t} + \frac{\partial (\overline{\varrho}_0 \widehat{\widehat{u}_i \widehat{u}_j})}{\partial x_j} = -\frac{\partial \widehat{\overline{p_2^*}}}{\partial x_i} + \delta_{i3} \widehat{\widehat{\varrho}}_2 g - \epsilon_{ijk} \overline{\varrho}_0 \widehat{\widehat{u}}_k f_j + H_{u_i} - \frac{\partial \widehat{\tau}_{ij}}{\partial x_j}. \tag{2.31}$$

Extracting the resolved stress $\mathcal{L}_{ij} = \overline{\varrho}_0 (\widehat{\widehat{u_i u_j}} - \widehat{\widehat{u}}_i \widehat{\widehat{u}}_j)$ then gives

$$\frac{\partial \overline{\varrho}_0 \widehat{\widehat{u}}_i}{\partial t} + \frac{\partial (\overline{\varrho}_0 \widehat{\widehat{u}}_i \widehat{\widehat{u}}_j)}{\partial x_j} = -\frac{\partial \widehat{\overline{p_2^*}}}{\partial x_i} + \delta_{i3} \widehat{\widehat{\varrho}}_2 g - \epsilon_{ijk} \overline{\varrho}_0 \widehat{\widehat{u}}_k f_j + H_{u_i} - \frac{\partial \widehat{\tau}_{ij}}{\partial x_j} - \frac{\partial \mathcal{L}_{ij}}{\partial x_j}. \tag{2.32}$$

Alternatively, application of the grid and test filters together to the continuous equations gives

$$\frac{\partial \overline{\varrho}_0 \widehat{\widehat{u}}_i}{\partial t} + \frac{\partial (\overline{\varrho}_0 \widehat{\widehat{u}}_i \widehat{\widehat{u}}_j)}{\partial x_j} = -\frac{\partial \widehat{\overline{p_2^*}}}{\partial x_i} + \delta_{i3} \widehat{\widehat{\varrho}}_2 g - \epsilon_{ijk} \overline{\varrho}_0 \widehat{\widehat{u}}_k f_j + H_{u_i} - \frac{\partial T_{ij}}{\partial x_j}, \tag{2.33}$$

where

$$T_{ij} = \overline{\varrho}_0 \left(\widehat{\widehat{u_i u_j}} - \widehat{\widehat{u}}_i \widehat{\widehat{u}}_j \right). \tag{2.34}$$

Comparison of Eqs.(2.32) and (2.33) gives the Germano identity,

$$\mathcal{L}_{ij} = T_{ij} - \widehat{\tau}_{ij}. \tag{2.35}$$

The dynamic procedure assumes that the same parameterisation that is used to parameterise the SGS stress at the grid filter level τ_{ij} can be used to model the test level stress T_{ij}. The test level stress for the Smagorinsky and mixed models are written as

$$T_{ij}^a = -2 \overline{\varrho}_0 C \widehat{\Delta}^2 \left| \widehat{\widehat{D}} \right| \widehat{\widehat{D}}_{ij} \widehat{C}_B, \tag{2.36}$$

and

$$T_{ij} = L_{ij}^{*T} - 2 \overline{\varrho}_0 C \widehat{\Delta}^2 \left| \widehat{\widehat{D}} \right| \widehat{\widehat{D}}_{ij} \widehat{C}_B, \tag{2.37}$$

respectively. Here $\widehat{C}_B$ is given by

$$\widehat{C}_B = \left(1 - \widehat{Ri}_{sgs} \right)^{1/2} \qquad \widehat{Ri}_{sgs} < 1 \tag{2.38}$$

$$\widehat{C}_B = 0 \qquad \widehat{Ri}_{sgs} \geq 1, \tag{2.39}$$

with the test level Richardson number given by

$$\widehat{Ri}_{sgs} = \frac{g/\theta_0 \, \partial \widehat{\widehat{\theta}}_v / \partial z}{Pr_{sgs} |\widehat{\widehat{D}}|^2}. \tag{2.40}$$

The test level modified Leonard term in the mixed model L_{ij}^{*T} is found by decomposing T_{ij}

in a manner similar to the decomposition of τ_{ij} (see Eq.(2.22)). Substituting $u_i = \widehat{\widetilde{u}}_i + u_i''$ into Eq.(2.34) gives

$$T_{ij} = L_{ij}^{*T} + C_{ij}^{*T} + R_{ij}^{*T}, \tag{2.41}$$

where the modified Leonard, cross and Reynolds terms at the test level are

$$L_{ij}^{*T} = \overline{\varrho}_0(\widehat{\widehat{\widetilde{u}_i}\widehat{\widetilde{u}_j}} - \widehat{\widehat{\widetilde{u}_i}}\,\widehat{\widehat{\widetilde{u}_j}}) \tag{2.42}$$

$$C_{ij}^{*T} = \overline{\varrho}_0(\widehat{\widehat{\widetilde{u}_i}u_j''} + \widehat{\widehat{u_i''}\widetilde{u}_j} - \widehat{\widehat{\widetilde{u}_i}}\,\widehat{\widehat{u_j''}} - \widehat{\widehat{u_i''}}\,\widehat{\widehat{\widetilde{u}_j}}) \tag{2.43}$$

$$R_{ij}^{*T} = \overline{\varrho}_0(\widehat{u_i''u_j''} - \widehat{u_i''}\,\widehat{u_j''}). \tag{2.44}$$

In Eqs.(2.36-2.44) we have again used the fact that we assume a horizontal test filter so that Eqs.(2.29-2.30) can be used to simplify the equations.

The decomposition shown in Eqs.(2.42-2.44) is different from that derived by Zang *et al.* (1993), who used a decomposition based on $u_i = \widetilde{u}_i + u_i'$ at both the grid and test level, rather than the form $u_i = \widehat{\widetilde{u}}_i + u_i''$ used here for the test level. As noted by Vreman *et al.* (1994), the latter is more consistent with the dynamic procedure since the test level stress should be written in terms of test filtered velocity components in order to make the test level parameterisations analogous to those used at the grid level.

Substituting the parameterisations for the subgrid scale stress τ_{ij} (Eq.(2.26)) and test level stress T_{ij} (Eq.(2.37)) into the Germano identity (Eq.(2.35)) gives

$$\begin{aligned}\overline{\varrho}_0(\widehat{\widetilde{u}_i\widetilde{u}_j} - \widehat{\widetilde{u}_i}\,\widehat{\widetilde{u}_j}) = \;& \overline{\varrho}_0(\widehat{\widehat{\widetilde{u}_i}\widehat{\widetilde{u}_j}} - \widehat{\widehat{\widetilde{u}_i}}\,\widehat{\widehat{\widetilde{u}_j}}) - 2\overline{\varrho}_0 C\widehat{\Delta}^2 \left|\widehat{\widehat{\widetilde{D}}}\right| \widehat{\widehat{\widetilde{D}}}_{ij}\widehat{C}_B \\ & -\overline{\varrho}_0(\widehat{\widetilde{u}_i\widetilde{u}_j} - \widehat{\widetilde{u}_i}\,\widehat{\widetilde{u}_j}) + 2\overline{\varrho}_0 C\Delta^2 \widehat{\left|\widetilde{D}\right|}\,\widetilde{D}_{ij}C_B.\end{aligned} \tag{2.45}$$

Removing the constant factor $\overline{\varrho}_0$, and contracting tensors using the least squares approach of Lilly (1992) gives an equation for the model coefficient in the dynamic mixed model,

$$C\Delta^2 = -\frac{< M_{ij}(\mathcal{L}_{ij}^* - H_{ij}) >}{< 2M_{kl}M_{kl} >}, \tag{2.46}$$

where

$$\mathcal{L}_{ij}^* = \widehat{\widetilde{u}_i\widetilde{u}_j} - \widehat{\widetilde{u}_i}\,\widehat{\widetilde{u}_j}, \tag{2.47}$$

$$M_{ij} = \alpha^2 \left|\widehat{\widetilde{D}}\right| \widehat{\widetilde{D}}_{ij}\widehat{C}_B - \left|\widetilde{D}\right| \widehat{\widetilde{D}_{ij}C_B}, \tag{2.48}$$

$$H_{ij} = (\widehat{\widehat{\widetilde{u}_i}\widehat{\widetilde{u}_j}} - \widehat{\widehat{\widetilde{u}_i}}\,\widehat{\widehat{\widetilde{u}_j}}) - (\widehat{\widetilde{u}_i\widetilde{u}_j} - \widehat{\widetilde{u}_i}\,\widehat{\widetilde{u}_j}), \tag{2.49}$$

α is the ratio of the test and grid filters

$$\alpha = \widehat{\Delta}/\Delta, \tag{2.50}$$

and $< >$ indicates averaging on horizontal planes. Equivalently, for the dynamic Smagorinsky model,

$$C\Delta^2 = -\frac{< M_{ij}\mathcal{L}_{ij}^{*a} >}{< 2M_{kl}M_{kl} >}. \tag{2.51}$$

The models outlined above use the original dynamic procedure of Germano *et al.* (1991) and require averaging in homogeneous directions to remain stable. Ghosal *et al.*

(1995) recast the dynamic procedure as a constrained variational problem and used this approach to develop a "dynamic localization model" that does not require averaging. This model, however, requires the solution of an integral equation and is computationally expensive. A less expensive alternative proposed by Piomelli & Liu (1995) involves finding an approximate solution to the integral equation by using the value of C at the previous time step to give a first approximation C^*. Applying their procedure gives localised versions of the models. The coefficient for the localised dynamic Smagorinsky model is given by

$$C = -\frac{(\mathcal{L}_{ij}^{*a} - 2\widehat{C^* B_{ij}})A_{ij}}{2A_{kl}A_{kl}}. \tag{2.52}$$

where,

$$A_{ij} = \alpha^2 \Delta^2 \left|\widehat{\widetilde{D}}\right| \widehat{\widetilde{D}}_{ij} \widehat{C}_B, \tag{2.53}$$

$$B_{ij} = \Delta^2 \left|\widetilde{D}\right| \widetilde{D}_{ij} C_B. \tag{2.54}$$

The coefficient for the localised dynamic mixed model is

$$C = -\frac{(\mathcal{L}_{ij}^{*} - H_{ij} - 2\widehat{C^* B_{ij}})A_{ij}}{2A_{ij}A_{ij}}, \tag{2.55}$$

with A_{ij} and B_{ij} given by Eqs.(2.53) and (2.54) respectively and H_{ij} given by Eq.(2.49).

We note here that by using a horizontal test filter we have reduced the complexity of our models considerably. With three-dimensional test filtering the models would be of similar complexity to the equivalent dynamic models for compressible flow whereas, when a horizontal filter is used, the models for the anelastic equations become similar to those for incompressible flow. In fact, if the discretisation operator is taken as being equivalent to the first level of grid scale Favre filtering (that is, we assume implicit filtering at the grid scale), then the only difference in the implementation occurs in the mixed model, where the second grid scale filter in the formula for H_{ij} (Eq.(2.49)) is a Favre filter that must be applied explicitly.

An interesting feature of the localised dynamic model is that, if unconstrained, it can calculate negative values for the model coefficient, and thus predict regions of negative eddy viscosity. While such regions may be interpreted as regions of backscatter, or energy transfer from small to large scales, Ghosal *et al.* (1995) and Carati *et al.* (1995) note that the dynamic Smagorinsky model has no information about how much energy is actually available in the subgrid scales. Consequently, there is no mechanism by which such a "counter-gradient diffusion" model for backscatter can be turned off once all the subgrid scale energy has been removed. For this reason we chose to clip the eddy viscosity at zero. For the localised model backscatter is therefore included. For the plane averaged dynamic Smagorinsky model, however, the effect of backscatter is included in an average sense through a reduction of the plane averaged model coefficient. As noted above, in the mixed model the Leonard term allows backscatter, so there is no need to resort to using a negative eddy viscosity.

The Smagorinsky and mixed models for the subgrid scale fluxes of the scalar variables

are written

$$\gamma_\phi = -\overline{\varrho}_0 C_\phi \Delta^2 \left|\widetilde{D}\right| \frac{\partial \widetilde{\phi}}{\partial x_j} C_B, \tag{2.56}$$

$$\gamma_\phi = \overline{\varrho}_0 (\widetilde{\widetilde{\phi}\widetilde{u}}_j - \widetilde{\widetilde{\phi}}\widetilde{\widetilde{u}}_j) - \overline{\varrho}_0 C_\phi \Delta^2 \left|\widetilde{D}\right| \frac{\partial \widetilde{\phi}}{\partial x_j} C_B. \tag{2.57}$$

Here ϕ is a generic scalar representing θ_l^* or q_t. The mixed model includes a term representing the scalar equivalent of the modified Leonard term,

$$L^*_{\phi j} = \overline{\varrho}_0 (\widetilde{\widetilde{\phi}\,\widetilde{u}}_j - \widetilde{\widetilde{\phi}}\,\widetilde{\widetilde{u}}_j). \tag{2.58}$$

Equations for the model coefficients are then written in a form analogous to that used for the subgrid scale stress. For the plane averaged dynamic Smagorinsky model,

$$C_\phi \Delta^2 = -\frac{< F_j E_j >}{< F_k F_k >}, \tag{2.59}$$

where the resolved flux E_j is given by

$$E_j = \widehat{\widetilde{\phi}\,\widetilde{u}}_j - \widehat{\widetilde{\phi}}\,\widehat{\widetilde{u}}_j, \tag{2.60}$$

and

$$F_j = \alpha^2 \left|\widehat{\widetilde{D}}\right| \frac{\partial \widehat{\widetilde{\phi}}}{\partial x_j} \widehat{C}_B - \widehat{\left|\widetilde{D}\right| \frac{\partial \widetilde{\phi}}{\partial x_j}} C_B. \tag{2.61}$$

For the dynamic mixed model,

$$C_\phi \Delta^2 = -\frac{< F_j (E_j - G_j) >}{< F_k F_k >}, \tag{2.62}$$

where

$$G_j = (\widehat{\widetilde{\widetilde{\phi}\widetilde{u}}_j} - \widehat{\widetilde{\widetilde{\phi}}}\,\widehat{\widetilde{\widetilde{u}}}_j) - (\widehat{\widetilde{\widetilde{\phi}}\,\widetilde{u}}_j - \widehat{\widetilde{\widetilde{\phi}}}\,\widehat{\widetilde{\widetilde{u}}}_j). \tag{2.63}$$

The coefficient for the localised dynamic Smagorinsky model is given by

$$C_\phi = -\frac{(E_j - \widehat{C^*_\phi Q}_j) P_j}{P_k P_k}, \tag{2.64}$$

where

$$P_j = \alpha^2 \Delta^2 \left|\widehat{\widetilde{D}}\right| \frac{\partial \widehat{\widetilde{\phi}}}{\partial x_j} \widehat{C}_B, \tag{2.65}$$

$$Q_j = \Delta^2 \left|\widetilde{D}\right| \frac{\partial \widetilde{\phi}}{\partial x_j} C_B. \tag{2.66}$$

The coefficient for the localised dynamic mixed model is

$$C_\phi = -\frac{(E_j - G_j - \widehat{C^*_\phi Q}_j) P_j}{P_k P_k}, \tag{2.67}$$

with P_j and Q_j given by Eqs.(2.65) and (2.66) respectively, and G_j given by Eq.(2.63).

Close to the rough surface at the bottom of the domain the size of the turbulent eddies decreases and the turbulence models described above do not give the correct dissipation.

The standard Smagorinsky model is over-dissipative while the dynamic models are under-dissipative. With the standard Smagorinsky model we use a damping function suggested by Mason (1994),

$$\frac{1}{\Delta^{*2}} = \frac{1}{\Delta^2} + \frac{1}{(k(z+z_0))^2}, \tag{2.68}$$

where k is the Von Kàrmàn constant and z_0 the roughness length. With all models we also add a surface layer stress term suggested by Brown *et al.* (2001). This stress takes the form

$$\tau_{sfc} = -\int C_{sfc} a(z) \rho_0 |\boldsymbol{u}| \phi dz, \tag{2.69}$$

where C_{sfc} is a scaling factor, a(z) a smoothing function, $|\boldsymbol{u}|$ the horizontal wind speed and ϕ the dependent variable. At present we follow Chow & Street (2002) and choose C_{sfc} to give τ_{sfc} equal to half the surface flux at the first grid point above the wall.

3. Simulation results

The test case chosen for the simulations is the first research flight (RF01) of the second Dynamics and Chemistry of Marine Stratocumulus (DYCOMS-II) field experiment. The computational domain extends 3.2km in the two horizontal directions and 1.5km in the vertical direction, with $96 \times 96 \times 128$ cells in the x, y and z directions respectively. Cell-spacing is uniform in the horizontal directions and stretched in the vertical direction to give cells of height 5m close to the bottom surface and in the vicinity of the inversion. This grid is typical of that currently used in large eddy simulations of the atmospheric boundary layer. The spatial discretisation uses a second-order centered scheme with no flux limiting, while time integration uses a second order Runge-Kutta scheme. The simulation is integrated over a period of four hours. Further details of the simulation set-up are described in Kirkpatrick *et al.* (2003) and will not be repeated here.

In the following we compare results obtained with four of the SGS turbulence models described above: the standard Smagorinsky (SM), dynamic Smagorinsky (DSM), dynamic mixed (DMM) and localised dynamic Smagorinsky model (LDSM). The standard Smagorinsky model uses a constant coefficient of $C_S = C^{1/2} = 0.18$ and a Prandtl number of $Pr_{sgs} = 0.4$. For reference, we also show results obtained with no SGS model.

Figure 1 shows vertical profiles of condensed water, liquid water potential temperature, eddy viscosity and diffusivities and SGS Prandtl number predicted by the various models. These profiles are calculated by averaging over horizontal planes as well as over a time period of 30 minutes. All profiles are calculated for the last half hour of the simulation, that is for $t = 3.5 - 4$h. The dynamic Smagorinsky models give quantitatively similar profiles to the standard Smagorinsky model. LDSM gives somewhat higher average eddy viscosity and diffusivities than DSM. This is because negative values of eddy viscosity predicted by LDSM are clipped, whereas with DSM conditions that would produce local negative values have the effect of reducing the plane average. The unclipped model coefficient profiles for DSM and LDSM (not shown) were found to be almost identical. The dynamic mixed model gives lower values of eddy viscosity and diffusivity because the Leonard term component of the SGS stress is included separately. All models predict a SGS turbulent Prandtl number close to the standard value of 0.4 through most the boundary layer, although DSM predicts an increase to a value of approximately 2 in the region just below the inversion. The reason for this behaviour, which is not seen with the other models, is not clear at present.

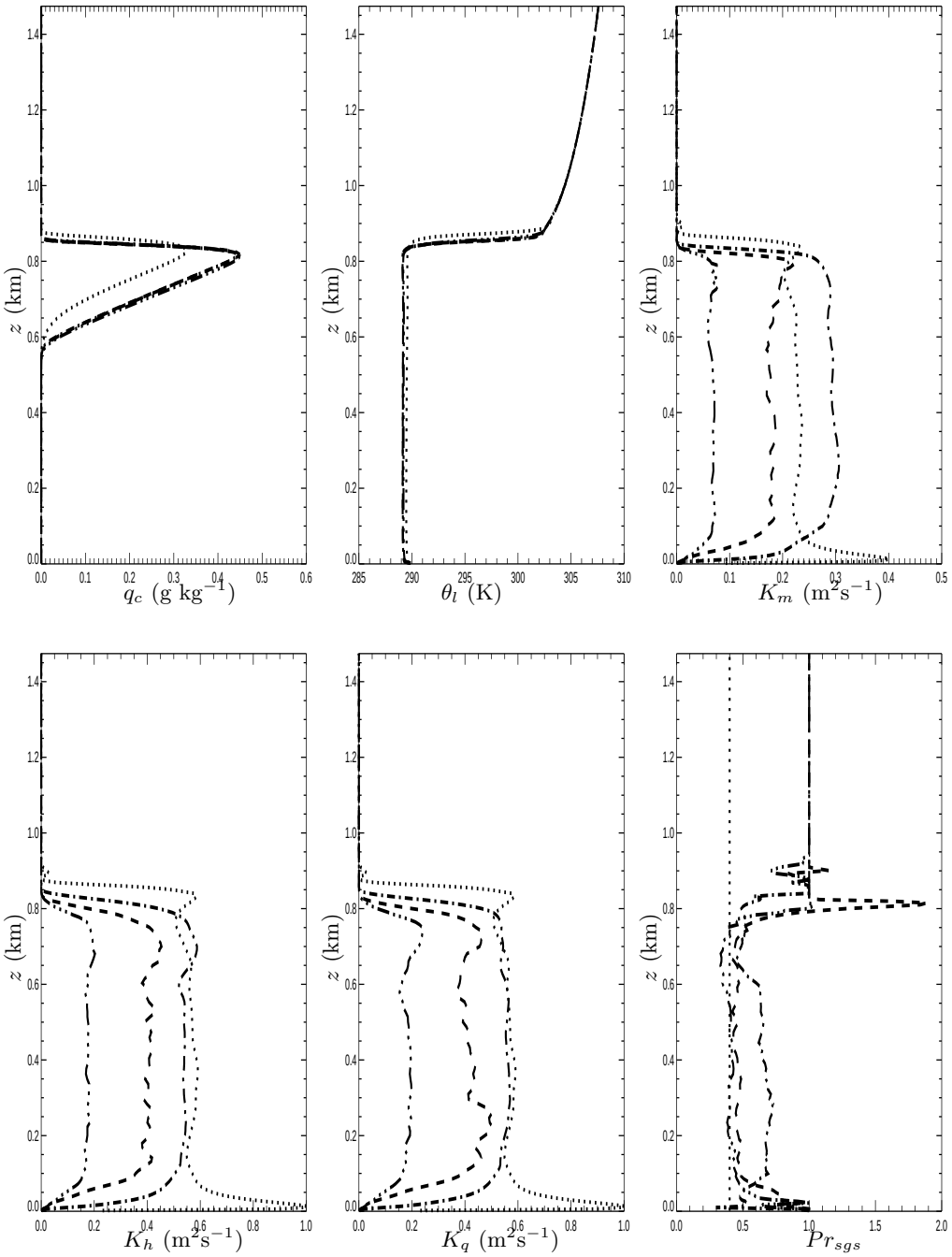

FIGURE 1. Vertical profiles of condensed water, liquid water potential temperature, eddy viscosity and diffusivities, and SGS Prandtl number: $\cdots$ SM, $- - -$ DSM, $- \cdot -$ LDSM, $- \cdots -$ DMM.

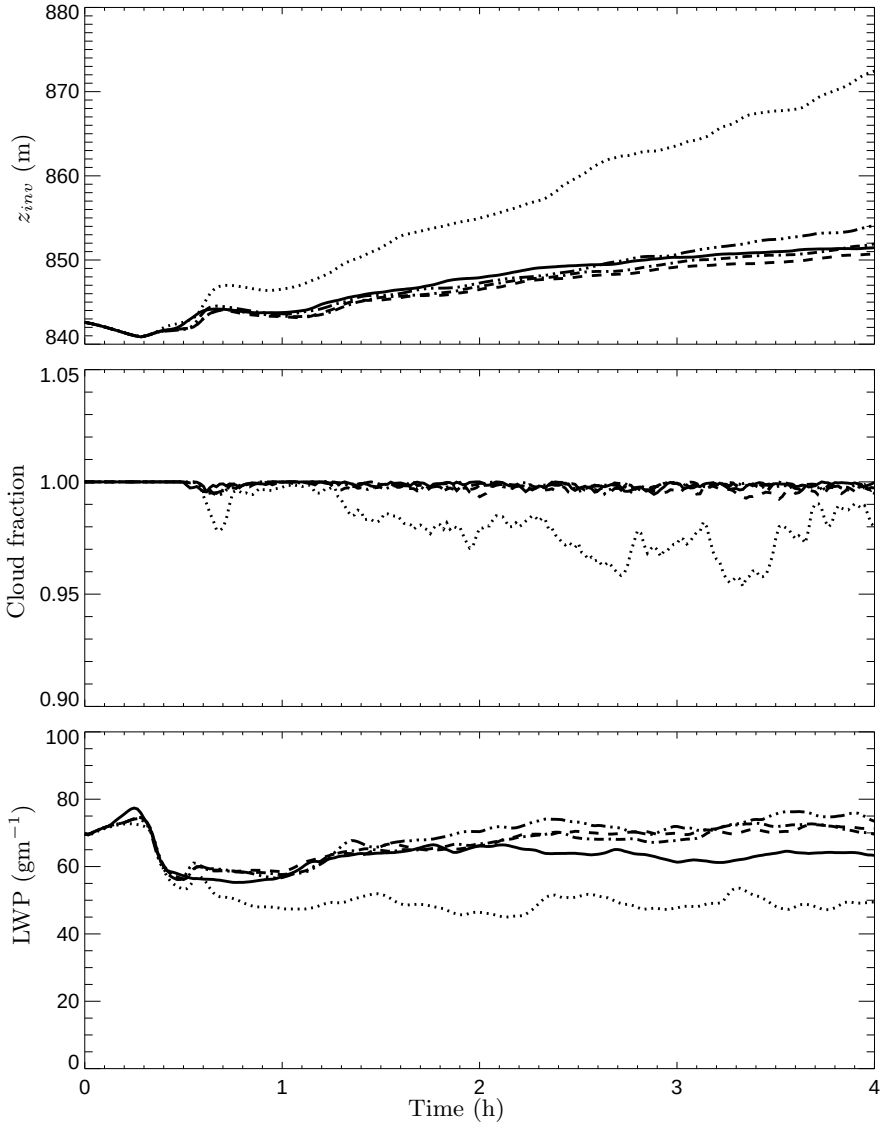

FIGURE 2. Time series of inversion height, cloud fraction and liquid water path: —— no SGS model, $\cdots$ SM, $-\,-\,-$ DSM, $-\cdot-$ LDSM, $-\cdots-$ DMM.

Figure 2 shows time series of inversion height z_{inv}, liquid water path LWP and cloud fraction. The entrainment rate E can be estimated from the rate of change of z_{inv} using the formula,

$$E = \frac{dz_{inv}}{dt} - w_{sub}. \tag{3.1}$$

Here w_{sub} is the subsidence velocity, which for the present case is estimated to be -0.3cms^{-1}. dz_{inv}/dt is calculated as the average rate of change over the period $t = 2-4$h. The dynamic Smagorinsky models give an entrainment rate of approximately 0.36-

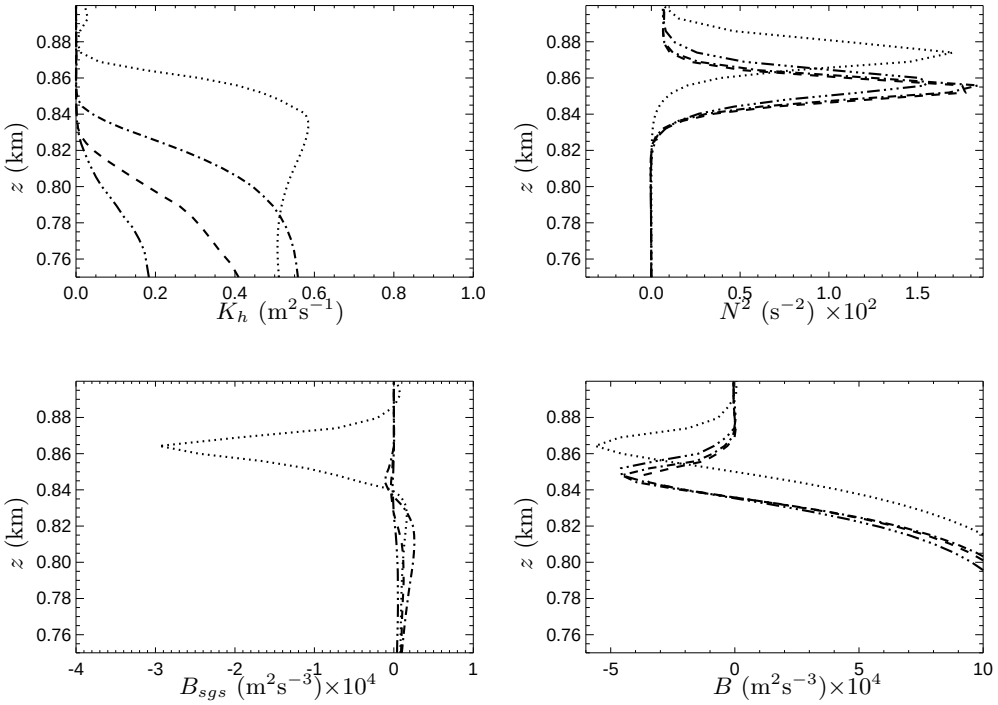

FIGURE 3. Eddy diffusivity, buoyancy frequency, and SGS and resolved buoyancy production at cloud-top: ··· SM, − − − DSM, − · − LDSM, − · · · − DMM.

0.37cms^{-1}, while the dynamic mixed model gives 0.40cms^{-1}. These results are in excellent agreement with the entrainment rate $E = 0.38 \pm 0.04$cms^{-1} estimated from observational measurements. The standard Smagorinsky model, however, overpredicts entrainment significantly giving $E \approx 0.55$cms^{-1}. The entrainment rate with no SGS model is 0.34cms^{-1}, which is slightly lower than that obtained with the dynamic models, but still within the error bounds of the observational measurements. The observed liquid water path and cloud fraction remained approximately constant during the experiment. This is also well predicted with dynamic models and no SGS model, while with the standard Smagorinsky model the results for these parameters again deviate significantly.

To help explain these differences, Figure 3 shows a comparison of the eddy diffusivity K_h, squared buoyancy frequency N^2, resolved buoyancy production B and subgrid scale buoyancy production B_{sgs}. Subgrid scale buoyancy production is approximated as

$$B_{sgs} \approx -K_h N^2. \tag{3.2}$$

The buoyancy frequency is calculated using a method described by Stevens *et al.* (2002). This approach is an extension of the work of MacVean & Mason (1990) and takes into account changes in stability that occur when subgrid scale mixing causes condensation or evaporation. Figure 3 shows the eddy diffusivity predicted by the standard Smagorinsky model decreasing through the inversion as a result of the stable stratification which drives the buoyancy correction coefficient C_B in the model to zero (see Eq.(2.16)). There is, however, a significant overlap region in which both the eddy diffusivity and buoyancy frequency are large. From Figure 3 and Eq.(2.16) it is clear that this overlap region

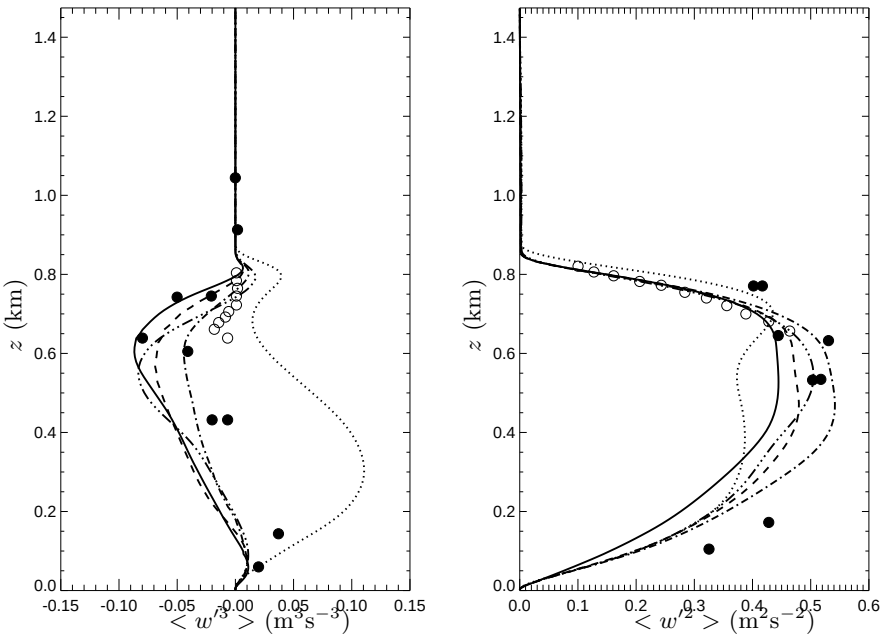

FIGURE 4. Second and third moments of vertical velocity. Simulation results (resolved component only): ——— no SGS model, ··· SM, − − − DSM, − · − LDSM, − · · · − DMM. Measurements: radar data (open circles), *in situ* measurements (filled circles).

also constitutes a zone of negative subgrid scale buoyancy production. Meanwhile the resolved buoyancy production with SM is similar to that seen with the other models. Negative buoyancy production is associated with conversion of mechanical energy into potential energy. In the present case this is interpreted as turbulence doing work to mix the warmer air above the inversion with cooler boundary-layer air below. Thus, the extra $-B_{sgs}$ provided by the standard Smagorinsky model is the cause of the enhanced entrainment rate seen with this model. Excessive entrainment of warm, dry air across the inversion then leads to the observed reduction of cloud fraction and liquid water path.

The same effect is not seen with the dynamic models which damp the model coefficient so that it becomes zero just *below* the inversion. Consequently there is no overlap region and no region of significant negative SGS buoyancy production. By coincidence, the same effect is also achieved when no SGS model is used, which explains the similarity between the results obtained with the dynamic models and no SGS model for large scale parameters such as entrainment rate, liquid water path and cloud fraction.

Figure 4 shows vertical profiles for the second and third moments of the resolved vertical velocity component compared with the observational measurements. The second moment is well predicted in the dynamic model simulations, with numerical results in excellent agreement with observations. The shape of the profiles obtained with the dynamic models is also typical of a well-mixed boundary layer as is expected for nocturnal stratocumulus. In contrast, the simulation using the standard Smagorinsky model does not agree as well with the observations and gives a two-peaked profile. Such a profile indicates a decoupling of the cloud layer and sub-cloud layer which is not apparent in the observational results.

The differences in profiles of the third moment are even more striking. The standard Smagorinsky model gives reasonable results in the surface layer, but does not give the negative values observed in the cloud layer. The dynamic models, on the other hand, give good agreement with the observations throughout the boundary layer, although, close to the surface they appear to under-predict the magnitude of this statistic somewhat. More work is required on the surface layer model to improve this.

4. Future work

The results presented in this paper clearly demonstrate the utility of dynamic turbulence models for atmospheric simulations. There is, however, much work still to be done. At present we are using a second-order accurate scheme for the spatial-discretisation. Consequently the numerical errors are of a similar magnitude to the terms associated with the subgrid scale models. The authors are currently working on a fourth-order scheme to resolve this issue. More work is also required in refining the surface layer model, especially where it is applied in combination with the dynamic models. As discussed above, dynamic models tend to underpredict the dissipation in the surface layer. This is because as the surface is approached the energetic eddies are no longer resolved and the assumptions underlying the dynamic procedure break down. While the current surface layer model helps to overcome these issues, the surface layer velocity and scalar profiles still deviate significantly from profiles predicted by similarity theory.

REFERENCES

Bardina, J., Ferziger, J. H. & Reynolds, W. C. 1980 Improved subgrid scale models for large eddy simulation. AIAA paper 80-1357.

Bardina, J., Ferziger, J. H. & Reynolds, W. C. 1983 Improved turbulence models based on large eddy simulation of homogeneous, incompressible, turbulent flows. *Tech. Rep.* TF-19. Stanford University, Thermosciences Division, Dept. of Mech. Engr.

Boivin, M., Simonin, O. & Squires, K. D. 2000 On the prediction of gas-solid flows with two-way coupling using large eddy simulation. *Phys. Fluids* **12**, 2080–2090.

Branley, N. & Jones, W. P. 2001 Large eddy simulation of a turbulent non-premixed flame. *Combust. and Flame* **127**, 1914–1934.

Brown, A. R., Hobson, J. M. & Wood, N. 2001 Large-eddy simulation of neutral turbulent flow over rough sinusoidal ridges. *Bound.-Layer. Meteorol.* **98**, 411–441.

Carati, D., Ghosal, S. & Moin, P. 1995 On the representation of backscatter in dynamic localization models. *Phys. Fluids* **7** (3), 606–616.

Chow, F. K. & Street, R. L. 2002 Modeling unresolved motions in LES of field-scale flows. In *15th Symposium on Boundary Layers and Turbulence, 15-19 July*.

Clark, T. L. 1979 Numerical simulations with a three-dimensional cloud model: Lateral boundary condition experiments and multicellular severe storm simulations. *J. Atmos. Sci.* **36**, 2191–2215.

Deardorff, J. W. 1972 Convective velocity and temperature scales for the unstable planetary boundary layer and Rayleigh convection. *J. Atmos. Sci.* **27**, 1211–1213.

Deardorff, J. W. 1974 Three-dimensional numerical study of turbulence in an entraining mixed layer. *Bound.-Layer. Meteorol.* **7**, 199–226.

Deardorff, J. W. 1980*a* Stratocumulus-capped mixed layers derived from a 3-dimensional model. *Bound.-Layer. Meteorol.* **18** (4), 495 – 527.

Deardorff, J. W. 1980*b* Stratocumulus-capped mixed layers derived from a three-dimensional model. *Bound.-Layer. Meteorol.* **18**, 495–527.

Germano, M. 1986 A proposal for a redefinition of the turbulent stresses in the filtered Navier-Stokes equations. *Phys. Fluids* **29** (7), 2323–2324.

Germano, M., Piomelli, U., Moin, P. & Cabot, W. H. 1991 A dynamic subgrid-scale eddy viscosity model. *Phys. Fluids* **A 3** (7), 1760–1765.

Ghosal, S., Lund, T. S., Moin, P. & Akselvoll, K. 1995 A dynamic localization model for large-eddy simulation of turbulent flows. *J. Fluid Mech.* **286**, 229–255.

Kirkpatrick, M. P., Ackerman, A. S., Mansour, N. N. & Stevens, D. E. 2003 Dynamic turbulence models for large-eddy simulations of the cloud-topped atmospheric boundary layer. In prep. for submission to J. Atmos. Sci.

Lilly, D. K. 1962 On the numerical simulation of buoyant convection. *Tellus* **14** (2), 148 – 172.

Lilly, D. K. 1992 A proposed modification of the Germano subgrid scale closure method. *Phys. Fluids* **A 4**, 633–635.

MacVean, M. K. & Mason, P. J. 1990 Cloud top entrainment instability through small-scale mixing and its parameterization in numerical models. *J. Atmos. Sci.* **47** (8), 1012–1030.

Martin, M. P., Piomelli, U. & Candler, G. V. 2000 Subgrid-scale models for compressible large-eddy simulations. *Theor. Comp. Fluid Dyn.* **13**, 361–376.

Mason, P. 1989 Large-eddy simulation of the convective atmospheric boundary-layer. *J. Atmos. Sci.* **46** (11), 1492–1516.

Mason, P. J. 1994 Large-eddy simulation: A critical review of the technique. *Quart. J. Royal Meteor. Soc.* **120** (515/pt.A), 1–26.

Ogura, Y. & Phillips, N. 1962 Scale analysis of deep and shallow convection in the atmosphere. *J. Atmos. Sci.* **19**, 173–179.

Piomelli, U. & Liu, J. 1995 Large eddy simulation of rotating channel flows using a localized dynamic model. *Phys. Fluids* **7**, 839–848.

Smagorinsky, J. 1963 General circulation experiments with the primitive equations, I. The basic experiment. *Mon. Weath. Rev.* **91**, 99–164.

Stevens, D. E., Ackerman, A. S. & Bretherton, C. S. 2002 Effects of domain size and numerical resolution on the simulation of shallow cumulus convection. *submitted to J. Atmos. Sci.* .

Stevens, D. E., Bell, J. B., Almgren, A. S., Beckner, V. E. & Rendleman, C. A. 2000 Small-scale processes and entrainment in a stratocumulus marine boundary layer. *J. Atmos. Sci.* **57** (4), 567–581.

Stevens, D. E. & Bretherton, C. S. 1999 Effects of resolution on the simulation of stratocumulus entrainment. *Quart. J. Royal Meteor. Soc.* **125** (554/pt.B), 425–439.

Vreman, B., Geurts, B. & Kuerten, H. 1994 On the formulation of the dynamic mixed subgrid-scale model. *Phys. Fluids* **6** (12), 4057–4059.

Zang, Y., Street, R. & Koseff, J. R. 1993 A dynamic mixed subgrid-scale model and its application to recirculating flows. *Phys. Fluids* **A 5** (12), 3186–3196.